Langmuir

Article

pubs.acs.org/Langmuir

Control of Membrane Permeability in Air-Stable Droplet Interface Bilayers

Prachya Mruetusatorn,[†,⊥] Georgios Polizos,[∥] Panos G. Datskos,[∥] Graham Taylor,[‡] Stephen A. Sarles,[‡] Jonathan B. Boreyko,[§,#,⊥] Douglas G. Hayes,[†] and C. Patrick Collier*[,⊥]

[†]Department of Biosystems Engineering & Soil Science, [‡]Department of Mechanical, Aerospace, and Biomedical Engineering, and [§]Bredesen Center for Interdisciplinary Research and Graduate Education, The University of Tennessee, Knoxville, Tennessee 37996, United States

[∥]Energy and Transportation Science Division and [⊥]Center for Nanophase Materials Sciences, Oak Ridge National Laboratory, Oak Ridge, Tennessee 37831, United States

[#]Department of Biomedical Engineering and Mechanics, Virginia Polytechnic Institute and State University, Blacksburg, Virginia 24061, United States

Supporting Information

ABSTRACT: Air-stable droplet interface bilayers (airDIBs) on oil-infused surfaces are versatile model membranes for synthetic biology applications, including biosensing of airborne species. However, airDIBs are subject to evaporation, which can, over time, destabilize them and reduce their useful lifetime compared to traditional DIBs that are fully submerged in oil. Here, we show that the lifetimes of airDIBs can be extended by as much as an order of magnitude by maintaining the temperature just above the dew point. We find that raising the temperature from near the dew point (which was 7 °C at 38.5% relative humidity and 22 °C air temperature) to 20 °C results in the loss of hydrated water molecules from the polar headgroups of the lipid bilayer membrane due to evaporation, resulting in a phase transition with increased disorder. This dehydration transition primarily affects the bilayer electrical resistance by increasing the permeability through an increasingly disordered polar headgroup region of the bilayer. Temperature and relative humidity are conveniently tunable parameters for controlling the stability and composition of airDIB membranes while still allowing for operation in ambient environments.

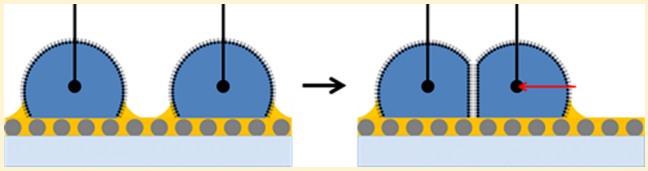

INTRODUCTION

A number of artificial lipid bilayer systems have been developed as models for cellular membranes, including supported lipid bilayers[1] and giant unilamellar vesicles.[2] Droplet interface bilayers (DIBs)[3] are useful model membrane systems that possess a number of attractive features for synthetic biology including robustness and stability,[4,5] tunable size and geometry,[6−8] ease of electrical characterization,[9−11] and incorporation of asymmetry into the bilayer.[12] Typically, DIBs are submerged in oil,[13] which precludes their use as detectors of airborne matter in ambient environments because material would have to traverse a thick layer of oil before encountering a membrane.

It was recently found that porous hydrophobic substrates can be infused with a lubricant to create a slippery surface for deposited droplets.[14−17] When two or more aqueous droplets meet on an oil-infused surface, the oil menisci that surround each droplet can merge spontaneously to form ultrathin oil layers between the droplets that prevent their coalescence (Figure 1(a)).[18] We showed that when amphiphilic lipid molecules were included in the aqueous droplets, air-stable lipid bilayers (airDIBs) replaced the thinning oil membranes. This enabled the electrical characterization of single alamethicin peptide ion channels inserted into the membrane.[18] AirDIBs are easy to manipulate and electrically characterize, which makes them good candidates for the biosensing of molecules in ambient environments. However, evaporation of water from the droplets caused the gradual separation of the bilayer due to the decrease in surface area shared by adjacent droplets as a result of the increase of the droplets' curvature. As a result, the useable lifetime of the airDIB system was reduced to about 20 min on average.[18] Although evaporation is not generally a serious problem for oil-submerged DIBs consisting of microliter-sized droplets, it does become problematic once the droplet size decreases to a point where surface-area-to-volume ratios become sufficiently large (femtoliter to picoliter scale) that the pervaporation of water into oil becomes significant.[19,20] As DIB volumes become increasingly smaller, methods for controlling evaporation rates that shorten useable lifetimes will have to be developed.

Here we describe the use of temperature control to delay the evaporation of water from airDIBs formed on oil-infused

Received: December 3, 2014
Revised: February 21, 2015

DOI: 10.1021/la504712g
Langmuir XXXX, XXX, XXX−XXX

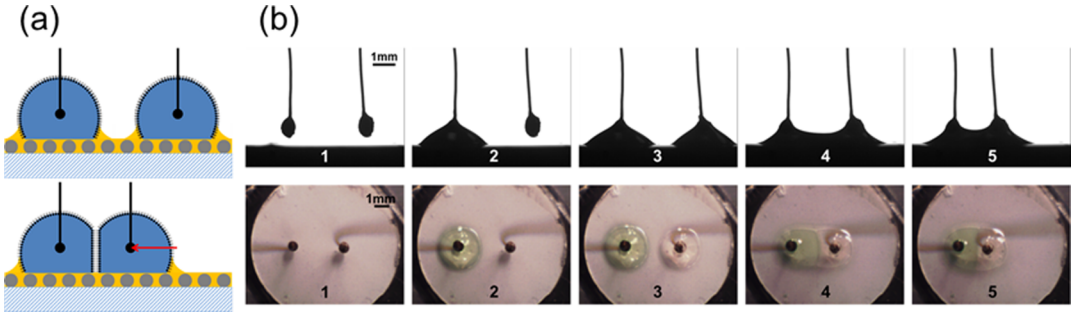

Figure 1. (a) Schematic of airDIB formation. Two droplets are brought together on an oil-infused superhydrophobic surface. The trapping of a thin oil film between the droplets prevents coalescence. (b) Side (top row) and top-down (bottom row) views of the sequence of steps involved in forming and manipulating an air-stable droplet interface bilayer (airDIB). Aqueous droplets containing lipids were pipetted onto two electrodes suspended just above the oil-infused superhydrophobic surface and brought together with a micromanipulator to form an airDIB. Green food coloring was added to one of the drops to aid contrast. Changing the temperature to just above the dew point (8 to 9 °C) lengthened the usable lifetime of airDIB by about an order of magnitude (Movies S1 and S2).

nanostructured surfaces that leads to bilayer rupture. We find that by keeping the temperature just above the dew point (per the atmospheric temperature and relative humidity conditions in our laboratory) to minimize evaporation while at the same time limiting condensation, the lifetime of the bilayer can be extended by more than an order of magnitude (4 h) compared to that at room temperature (20 min). When the temperature difference between the airDIB and the dew point was increased, a simultaneous decrease in both nominal bilayer capacitance and resistance occurred, which was unexpected because resistance and capacitance should have opposite dependencies on bilayer area.[21,22] Evaporation led to increased disorder in membrane packing, related to the loss of water molecules of hydration from the polar headgroup region of the bilayer. The increased disorder in turn lowers the energy barrier for ion transport across the membrane by disrupting the highly structured electric double layer, resulting in a lowered resistivity (membrane resistance). While a decrease in specific capacitance (per unit area) has been reported at increased temperatures for bilayer membranes,[23−26] the decrease in resistivity resulting from the evaporation of membranes in general, including both oil-submerged DIBs and airDIBs, is new.

MATERIALS AND METHODS

Superhydrophobic Nanostructured Glass Fabrication. Fumed silica functionalized with hexamethyldisilazane (commercial name, Aerosil R8200) was purchased from Evonik Industries (Essen, Germany) and was used as received. Colloidal silica (lot no. 100607, Nissan Chemical, Houston, TX) was functionalized in a solution of hexane and tridecafluoro-1,1,2,2-tetrahydrooctyl trichlorosilane (Gelest Inc., Morrisville, PA). The concentrations of the colloidal silica and silane in hexane were 10 and 1 wt %, respectively. The solution was stirred for 8 h at room temperature. The retrieved powder was washed with ethanol to remove unreacted silane groups and then dried at 60 °C for 24 h. The functionalized colloidal silica and fumed silica were suspended in 20 g of isopropyl alcohol, 3 g of 4-chlorobenzotrifluoride (PCBTF), and 3 g of urethane polymer resin. The suspension was ultrasonically agitated for 1 h and subsequently was spun at 1000 rpm for 30 s (Speedline Technologies G3-8 centrifuge, Specialty Coating Systems, Indianapolis, IN) on 10-mm-diameter round glass substrates (Ted Pella Inc., Redding, CA). The water contact angle values on the superhydrophobic substrates were greater than 160° (Figure S1). The advancing and receding contact angles were 165 and 153°, respectively.

Infusing Oil and Aqueous Droplet Solution Preparation. Because the freezing point of hexadecane (18 °C) is higher than the dew-point temperature in our laboratory (7 °C), a 9:1 (v/v) ratio of AR 20 silicone oil (freezing point −70 °C, Sigma-Aldrich, St. Louis, MO) to hexadecane was used as the infusing oil for bilayer formation between droplets. The oil was uniformly spun on 10-mm-diameter superhydrophobic glass substrates at 750 rpm for 45 s. The low viscosity of the mixture ensured that the initial oil film between the two droplets will rapidly drain and become replaced by a droplet interface bilayer. The vesicle−buffer solutions consisted of 2 mM 1,2-diphytanoyl-*sn*-glycero-3-phosphocholine (DPhPC) phospholipids (Avanti Polar Lipids, Alabaster, AL) suspended in a 100 mM NaCl solution (Sigma). The vesicle solutions were prepared at room temperature by dissolving dried DPhPC lipids in deionized water. To prepare unilamellar liposomal suspensions with a low polydispersity, a modified protocol based on the large unilamellar vesicles by an extrusion technique (Avanti Polar Lipids) was used. The hydrated lipid suspension was subjected to four freeze/thaw cycles between −20 and +20 °C to increase the entrapment efficiency of water-soluble compounds. Once the mixture was completely hydrated, it was then extruded through 0.1-μm-pore-size membranes to obtain unilamellar liposomal suspensions.

Air-Stable DIB Formation. The oil-infused superhydrophobic glass substrate was thermally bonded with thermal paste onto a water-cooled Peltier stage (Deben MK3 Coolstage, Deben UK Ltd., Suffolk, United Kingdom), which was used to vary the temperature of the airDIBs from 1 to 20 °C. (To minimize the time required to reach a new temperature, set points were changed at the stage controller as single-step transitions.)

All experiments were performed in a class 1000 clean room with an ambient temperature of 22 ± 0.5 °C and a relative humidity of 38.5 ± 2.5% (corresponding to a dew-point temperature of 7 °C). Agarose-coated Ag/AgCl electrodes (125 μm diameter, Goodfellow, Coraopolis, PA) were positioned about 0.4 mm above the oil-infused superhydrophobic glass surface and separated from each other to prevent the aqueous droplets from merging prematurely (Figure 1(b), first frame). A droplet was deposited on the agarose-functionalized tip of each electrode such that it bridged the gap between the tip and the functionalized glass surface (Figure 1(b), second and third frames). A sufficient duration (7−10 min) was allocated for the self-assembly and stabilization of lipid monolayers along the droplet periphery to occur (Figure 1(b), third frame). The formation of lipid monolayers on the substrate surface and the aqueous droplets resulted in a decrease in the contact angle for the droplets with time. However, the agarose-coated electrode tips held the droplets above the substrate surface, limiting the extent of droplet wetting. The droplets were then brought together slowly and gently using a three-axis micromanipulator (World Precision Instruments, Inc., Sarasota, FL). Once the oil menisci of the opposing droplets overlapped, the droplets migrated toward each other because of surface tension (Figure 1(b), fourth frame). As the droplets merged, an ultrathin film of oil migrated upward between the droplets, effectively preventing coalescence. As the oil film drained away, it was replaced by a stable bilayer. Because of the effects of

DOI: 10.1021/la504712g
Langmuir XXXX, XXX, XXX−XXX

gravity and interactions with the substrate surface, electrodes, and each other at the bilayer membrane, the droplets were flattened vertically and stretched axially from spherical to resemble ellipsoids. The droplet interface area could be changed isothermally by using the micromanipulator to adjust the separation between the two electrodes (Figure 1(b), fifth frame). Two digital charge-coupled device (CCD) cameras were used to capture images of the airDIB droplets, one from the side (using the camera on a Ramé-Hart model 590 goniometer, Ramé-Hart Instrument Co., Succasunna, NJ) and one from above (Moticam 2500, Motic Instruments, Inc., Richmond, BC, Canada), in order to estimate changes in bilayer area and droplet volume with respect to changes in temperature or in separation distance between the electrodes. To estimate the droplet volume from camera images, each droplet was modeled as one-half of a triaxial ellipsoid with semiprincipal axes a, b, and c using ImageJ software[27] (Figure S2).

$$V = \frac{2\pi}{3}abc \qquad a > b > c \tag{1}$$

The area of the bilayer membrane between the drops was estimated by approximating the membrane as an ellipse, with major horizontal radius a and minor vertical radius b (Figure S3).

$$A = \pi ab \tag{2}$$

The segmented line tool in ImageJ was used to approximate the arc length of the curved membrane as the sum of several smaller line segments. The bilayer area was calculated as one-fourth the product of this total length and the height of the bilayer.

Electrical Measurements. Stable droplet interface bilayers were electrically characterized by measuring the current induced by a triangle-waveform voltage of 20 mV, 10 Hz (model 33522A function generator, Agilent, Santa Clara, CA) applied to two wire-type silver–silver chloride electrodes (125 μm diameter) with an agarose-coated ball at the tip of each electrode inserted into each droplet. The resulting current was recorded at 20 kHz using an Axopatch-1D patch-clamp amplifier (Axon Instruments Inc., Molecular Devices, Union City, CA) and a LabTrax-4/16 four-channel data acquisition device (World Precision Instruments). The formation of the bilayer could be verified by the growth of the capacitive current amplitude as a function of time as the intermediate oil film drained away (within 5 min, Figure S4). For most cases, the bilayer thickness (H_b) was assumed to be approximately constant (~6 ± 1 nm for DPhPC).[4,28] The nominal electrical capacitance (SI) and resistance of the lipid bilayer were determined by fitting the measured square-waveform current data with an equivalent electrical circuit model using custom scripts in Matlab.[29] All measurements were made within a customized Faraday cage for electrical shielding.

RESULTS AND DISCUSSION

Figure 2 shows the difference in the decay rate of bilayer capacitance at two different temperatures, 20 and 9 °C, which was 2 °C higher than the dew-point temperature in our clean room (38.5% relative humidity). Figure S5 consists of corresponding side and top views of the airDIBs at different times to compare the extent of water loss due to evaporation at these two temperatures. The bilayer at 20 °C had unzipped completely by 1500 s due to the loss of droplet volume whereas the bilayer at 9 °C was still intact at 9000 s. Lowering the temperature further to 8 °C gave the longest bilayer lifetime, up to 4 h (an order of magnitude enhancement) but also resulted in the condensation of water on the substrate. Real-time feedback control of temperature and/or relative humidity could be used to extend the lifetimes even further.

We then explored varying the temperature between 9 and 1 °C and between 9 and 20 °C. In both cases, the Peltier stage reached the new set-point temperature within 10 ± 2 s. Neglecting the interfacial thermal resistance between the superhydrophobic glass substrate and the water droplets, the

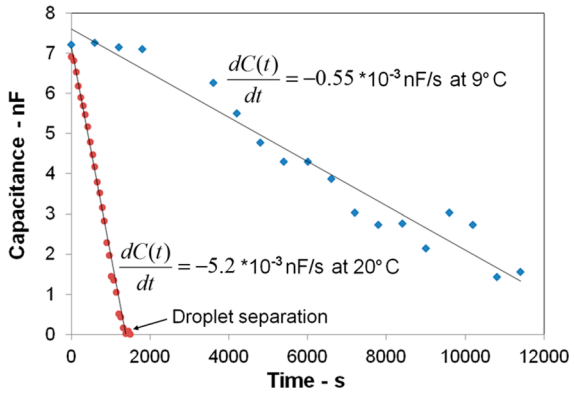

Figure 2. Effect of temperature on the rate of change of capacitance for airDIBs at 9 °C (blue diamonds) and 20 °C (red circles, see Movies S7 and S8).

time required for the airDIBs to equilibrate at the new set-point temperature given to the Peltier controller was about 2 s (SI), much faster than the time required for observable changes in the electrical properties of the membrane (several seconds to a few minutes).

Decreasing the temperature from 9 to 1 °C did not result in reproducible changes in bilayer capacitance or resistance, most likely due to the irreproducible nucleation and growth of condensate drops, followed by coalescence with the airDIB droplets (Movies S9 and S10). This prevented the use of swelling of airDIBs droplets below the dew point in order to rehydrate the bilayer. However, increasing the temperature from 9 to 20 °C did give reproducible results. This temperature shift consistently resulted in the bilayer capacitance and resistance both decreasing with time as the droplet volume decreased from evaporation, as shown in the top-down and side-view images in Figure 3. This result was unexpected

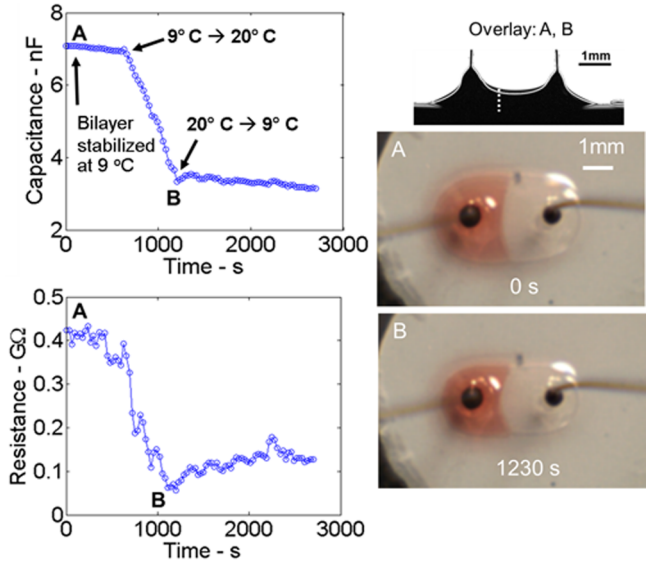

Figure 3. Effect of temperature on the capacitance and resistance of airDIBs versus time at 9 and 20 °C (left side) and corresponding side-view overlay (solid white line) and top-down views (right side). For thermal tuning of the bilayer, the electrode positions did not change (Movies S5 and S6). Because the bilayer is not visible in the side-view image, a dashed line has been added to the side-view image to indicate the approximate location of the bilayer.

DOI: 10.1021/la504712g
Langmuir XXXX, XXX, XXX−XXX

because nominal capacitance, (C), and resistance, (R), should have opposite dependencies on bilayer area, A, assuming that the thickness or composition of the bilayer did not change,[23−26]

$$C = \frac{\varepsilon A}{d} \tag{3}$$

$$R = \frac{\rho d}{A} \tag{4}$$

where ε is the dielectric permittivity of the bilayer, ρ is the resistivity, and d is the bilayer thickness. Figure 3 shows that once the temperature was returned to 9° from 20 °C, the rapid decay of capacitance and resistance returned to the same, much slower rates of decline seen at the beginning of the experiment. However, C and R did not return to their initial values.

By moving one of the electrodes relative to the other, the bilayer area could be mechanically modulated at a constant temperature of 9 °C. This measurement serves as a control for changes in capacitance and resistance in the bilayer due solely to isothermal changes in bilayer area, largely free from evaporation effects. Figure 4 shows how changing the electrode

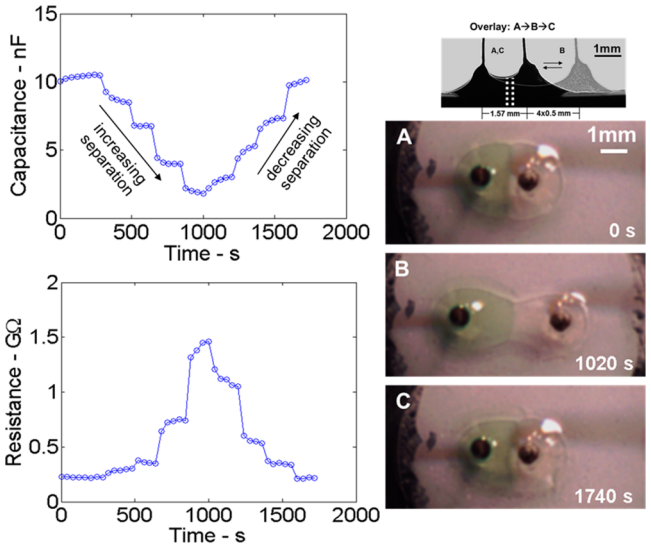

Figure 4. Effect of mechanical manipulation of the droplets' surface area on the capacitance and resistance of airDIBs versus time at 9 °C. Droplets were mechanically manipulated by moving one electrode relative to the other one over one cycle of several 0.5 mm steps (left side) and corresponding side-view overlay and top-down views (right side) (Movies S3 and S4). The dashed white lines in the side-view image are estimates of the locations of the bilayer as the separation distance between the droplets was varied between positions A (or C) and B.

separation in 0.5 mm steps affected the electrical properties of the bilayer. Similar behavior was seen over several cycles consisting of a single larger (1.5 mm) step (Figure S6). In contrast to the electrical behavior seen when the temperature was varied (Figure 3), mechanically tuning the bilayer area at constant temperature resulted in nominal capacitance and resistance values with opposite dependencies on bilayer area, consistent with expected trends (eqs 3 and 4). In contrast to the irreversibility of thermally driven changes, mechanical tuning of the bilayer resulted in reversible changes to the bilayer.

In Figure 5, capacitance values for both thermal and mechanical modulation of the bilayer in airDIBs are plotted

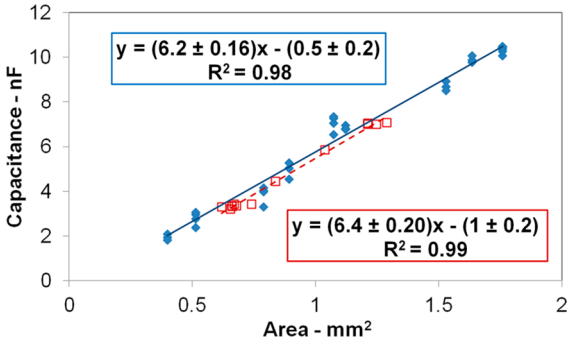

Figure 5. Capacitance versus area plots for mechanically tuned (blue diamonds) and thermally tuned (cycled between 9 and 20 °C (red unfilled squares)) airDIBs, corresponding to Figures 3 and 4. The slopes of the lines (mean value 0.63 ± 0.02 μF/cm^2), corresponding to the specific capacitances under these two conditions, were identical within the experimental uncertainty in the measurements, suggesting that changes in capacitance at elevated temperature were due primarily to the progressive loss of bilayer area as the two droplets that made up the airDIB lost volume during evaporation.

versus the changing bilayer area. The slope of such a plot gives the specific capacitance per unit area and is used to characterize the intrinsic dielectric properties of the bilayer separate from simple changes in area. The capacitance versus area plots for both cases were identical within the experimental uncertainty (mean slope value 0.63 ± 0.02 μF/cm^2), suggesting that the decrease in capacitance over this temperature range was due more to the progressive loss of bilayer area than to changes in membrane composition or thickness.[30] This value nearly matched the average specific capacitance (0.65 ± 0.048 μF/cm^2) obtained in control experiments with DPhPC DIBs submerged in the same oil mixture (9:1 AR20 silicone oil/hexadecane) (Figure S7).

The capacitances of the nonpolar, hydrophobic tail region ($\varepsilon \approx 2$)[31] and the polar headgroup region ($\varepsilon \approx 30$)[32] of the DPhPC bilayer are in series

$$\frac{1}{C_{tot}} = \frac{1}{C_{tails}} + \frac{1}{C_{heads}} \tag{5}$$

which means that the overall capacitance will be dominated by the smallest capacitance of the system, that of the hydrophobic tail region of the bilayer. This observation, along with the result depicted in Figure 5 which shows that both thermal and mechanical manipulation resulted in the same value for the specific capacitance, indicates that resistance is more sensitive than capacitance to changes in membrane composition or thickness due to evaporation. Furthermore, these changes affect the polar, hydrophilic headgroups of the bilayer primarily, not the nonpolar, hydrophobic tail region. Whereas the specific capacitance remained independent of bilayer area changes, the resistivity, ρ, which also should have been independent of area as long as the dielectric properties of the membrane had not been altered, displayed a 6-fold decrease as the temperature was increased to 20 °C. Upon returning to 9 °C, a very limited incomplete recovery of the resistivity was observed even as the bilayer area continued to decrease, which corroborates the hypothesis that the processes involved in changing the inherent membrane resistivity when the temperature is increased from 9 to 20 °C at 38.5% ambient relative humidity are, for the most part, irreversible (Figure S8).

DOI: 10.1021/la504712g
Langmuir XXXX, XXX, XXX−XXX

These observations are consistent with a dehydration-induced phase transition that affects the polar headgroup region of DPhPC bilayers. X-ray, neutron diffraction, and solid-state NMR studies have shown that water molecules can be sequestered within the interstitial spaces between the phosphatidylcholine headgroups of PC lipid membranes, including DPhPC membranes.[33,34] This confined internal water, known as hydrated water, has different thermodynamic and structural properties than bulk water because of differences in hydrogen-bonded networks with the headgroups compared to those in bulk water.[35] Osmotic stress experiments, which involve decreasing the ambient water activity of stacked lipid bilayer films by decreasing the relative humidity, have shown that DPhPC lipids undergo a liquid condensed to liquid expanded (L_α to L_α') phase transition primarily affecting the polar headgroup region of DPhPC bilayers. This region becomes increasingly disordered because of the expulsion of water molecules that can form coordinating hydrogen-bonded bridges between adjacent headgroups.[36,37] The resistivity of the DPhPC membrane is sensitive to the ordering of the headgroup region. The reorientation of the charged (zwitterionic) phosphatidylcholine headgroups in DPhPC with dehydration disrupts the highly structured electric double layer at the membrane, resulting in increased lateral heterogeneity at the interface and a higher permeability of the bilayer to ions (i.e., a lowered resistance).[38,39]

The driving force for this dehydration-induced phase transition of the membrane is the chemical potential of water, which may be thought of as the energy released when 1 mol of water is removed from the bilayer

$$\Delta\mu_w = RT \ln\left(\frac{\mathrm{RH}}{100}\right) \tag{6}$$

where R is the universal gas constant (0.08206 L atm/mol K), T is the absolute temperature (in Kelvin), and RH is the relative humidity, defined as the ratio of the partial pressure of water vapor in an air mixture and the saturated (equilibrium) water vapor pressure at that temperature:[33]

$$\mathrm{RH}_{\mathrm{lab}} = \left(\frac{p_w(T)}{p_{w,0}(T)}\right) \times 100\% \tag{7}$$

The chemical potential can be controlled with osmotic stress by adjusting the relative humidity and/or temperature of the ambient environment. We control the RH at the DIB sample surface by controlling the temperature of the aqueous droplets on the Peltier stage:

$$\mathrm{RH}_{\mathrm{sample}} = \mathrm{RH}_{\mathrm{lab}} \times \left(\frac{p_{w,0}(T_{\mathrm{lab}})}{p_{w,0}(T_{\mathrm{sample}})}\right) \tag{8}$$

Osmotic pressures corresponding to the chemical potentials acting on the water molecules in the bilayer are given by

$$\Pi = -\frac{\Delta\mu_w}{V_w} \tag{9}$$

where V_w is the partial molar volume of the water molecules in the bilayer. In the bulk, V_w is 30 Å^3 per molecule (18 mL/mol), although in the bilayer V_w will likely be less because of excluded volume considerations.[40,41] Figure S9 plots the chemical potential and the corresponding values of the osmotic pressure acting on water molecules in the bilayer as functions of RH and temperature. Values of Π ranging from 10^7 to 10^8 Pa (10^2 to 10^3 atm) represent strong driving forces for removing water molecules from the bilayer at low RH. Table 1 lists the effective relative humidity at the DIBs sample, and the corresponding chemical potential and osmotic pressure at the two temperatures featured in Figure 3. Increasing the sample temperature from 9 to 20 °C resulted in increases in the chemical potential and osmotic pressure by almost a factor of 5.

Table 1. Comparison of Chemical Potentials and Osmotic Pressures for the Two Droplets in Figure 3 at 9° C (Figure 3A) and at 20° C (Figure 3B)

T_{lab} = 22 °C, $\mathrm{RH}_{\mathrm{lab}}$ = 38.5% (dew point = 7 °C)	t = 0s, T = 9 °C	t = 1230s, T = 20 °C
$\mathrm{RH}_{\mathrm{sample}}$	83%	44%
$\Delta\mu_w$	−0.42 kJ/mol	−2.03 kJ/mol
Π	0.24×10^8 Pa	1.12×10^8 Pa

Another possible mechanism that could explain the drop in resistance in Figure 3 involves the buildup of osmotic pressures in the aqueous solution of the drops due to the presence of electrolytes. In this case, the osmotic pressures are given by the expression

$$\Pi = iMRT \tag{10}$$

where i is the van't Hoff factor (2 for NaCl) and M is the molarity of the salt solution in the drop. As a control, we added increasing amounts of NaCl to one of the droplets while maintaining the droplet temperature at 9 °C and looked for changes in the resistance behavior of the DIBs reminiscent of the thermally driven changes seen in Figure 3. Whereas the osmotic pressure due to increasing salt concentrations in the droplets increased by almost a factor of 2 (SI), the values (<10 atm) were still orders of magnitude less than the 10^2 to 10^3 atm range of osmotic pressure values caused by the external RH.

The increase in membrane curvature seen by the top-down camera during dehydration could modify the packing for the phospholipids residing at the interface, further increasing membrane permeability. However, the Laplacian pressure associated with the evaporative water loss would be small ($\sim 10^{-3}$ atm) due to the large radii of curvature (4.8 mm for droplet 1 and 3.1 mm for droplet 2), and is therefore not as important of a factor.

Other alternatives to a dehydration transition mechanism for increasing disorder in DPhPC lipids include direct heating. It is known that the area per DPhPC lipid increases with temperature,[34] and in general, lipid films can undergo a liquid-condensed to liquid-expanded phase transition with heating at constant RH or with a decrease in RH at constant temperature.[42] However, a consideration of the Π−T phase diagram specifically for DPhPC suggests that the L_α to L_α' transition cannot occur over the temperature range of 9 to 20 °C unless accompanied by a change in RH.[33] Regardless of how the phase transition occurred (change in temperature only, RH only, or some combination), it occurred over much longer time scales (30 s to a few minutes) than the time required for the temperature to equilibrate in the droplets (2 s, SI).

Another parameter that could affect R and C is the amount of oil in the membrane. It has been shown from specific capacitance measurements that hexadecane can partition into the DPhPC lipid tail region for up to 9.2% by volume, thereby increasing the effective bilayer thickness,[26] and that this effect

DOI: 10.1021/la504712g
Langmuir XXXX, XXX, XXX−XXX

increases with temperature.[30] This would imply that R would also increase with heating from 9 to 20 °C (per eq 3); however, the opposite trend occurred (Figure 3). These findings support our interpretation that the changes in R in the bilayer are primarily the result of dehydration of the headgroup regions, driven by evaporation at lower RH values. Other effects such as thermal fluctuations or oil intake in the tail region, while still likely to occur to some extent, seem to play secondary roles.

The fact that the decrease in R with an increase in temperature was not reversed upon a subsequent cooling cycle is consistent with an increase in entropy during heating resulting from the loss of water molecules associated with the phosphatidylcholine headgroups. Whether a phospholipid bilayer undergoes an increase or decrease in entropy during a dehydration-induced phase transition will ultimately depend on the changes in the hydrogen-bonded network within the interfacial region. 1,2-Dimyristoyl-*sn*-glycero-3-phosphocholine (DMPC) bilayers, which, unlike DPhPC, do not have the branched methyl groups on the hydrocarbon chains, undergo a decrease in entropy during dehydration as a result of a phase transition from a liquid crystalline to a more ordered gel phase.[33] These differences can be seen from the Π vs T phase diagrams of the two lipids. For DMPC bilayers, the slope of the $d\Pi/dT$ phase boundary is positive, corresponding to lower entropy for the dehydrated phase in accordance with the Clausius−Clapeyron equation,

$$\left(\frac{d\Pi}{dT}\right)_{\text{phase boundary}} \propto S_{\text{hydrated}} - S_{\text{dehydrated}} \tag{11}$$

whereas the opposite is true for DPhPC bilayers, which have a negative slope at the phase boundary, corresponding to a dehydrated phase that is less ordered.[33]

These considerations give clues that aid in understanding how changes in the extent of hydration or dehydration can alter the composition and permeability of lipid bilayers, impacting membrane resistance measurements. In contrast to DPhPC, the DMPC electrical conductivity increases (and resistance decreases) with hydration.[43] A useful parameter for understanding the differences in the behavior of lipid bilayers is the ratio of the area of the headgroup, A_{hg}, relative to that of the hydrocarbon chains, A_{ch}.[44] For DPhPC, steric repulsion of the methyl branches on the tails prevents efficient packing of the acyl chains, resulting in the formation of free-volume pockets for trapping water molecules, neutral solutes, and hydrated ions, along with a small A_{hg}/A_{ch} ratio. Variation of the A_{hg}/A_{ch} ratio with the state of hydration for DPhPC bilayers is governed primarily by headgroup energetics, not by thermodynamic changes in the tails. This is opposite to the case for DMPC bilayers, which have a larger A_{hg}/A_{ch} ratio governed chiefly by thermal fluctuations of the tail conformations.

The disruption of the polar headgroup regions of DPhPC bilayers during evaporation allows for the increased availability of interstitial space in the hydrophobic tail region for the solubilization of water and solutes, where they can dissolve (with solubility limited by the partition coefficient of molecules in the nonpolar environment) and cross the membrane by diffusion or migrate along defects containing hydrogen-bonded water molecules large enough to accommodate them.[37] In either case, the material composition and hence the dielectric constant of this region, ε, would not need to change significantly to support increased permeation rates and thereby increased conduction.

CONCLUSIONS

Air-stable droplet interface bilayers consisting of DPhPC lipids can experience an irreversible evaporation-induced dehydration transition which disrupts the integrity of the hydrated polar headgroup region of the membrane. An increase in electrical conductivity occurs due to the increased permeability of hydrated ions across the membrane, but membrane capacitance, which is dominated by the capacitance of the nonpolar hydrocarbon chains, is not significantly affected. This behavior is fundamentally different from the manipulation of the membrane by mechanical separation of the droplets, where the conductivity scales simply with membrane area. Temperature and relative humidity are attractive parameters for controlling the stability and composition of airDIB membranes. Although evaporation reduces the usable lifetime of airDIBs, evaporation rates can be decreased by up to an order of magnitude by lowering the temperature to a value near the dew-point temperature or, equivalently, by increasing the relative humidity. The choice to prevent evaporation by cooling the droplets to near the dew point was a matter of experimental convenience. For applications where room temperature (or higher) is desired, evaporation could be prevented at any system temperature by maintaining 100% relative humidity locally around the airDIBs in a temperature- and humidity-controlled cell.[45]

ASSOCIATED CONTENT

Supporting Information

Nanostructured surface characterization, determination of droplet volumes, determination of membrane areas, bilayer capacitive currents, images of thermally tuning airDIBs, determination of thermal equilibration times, images of mechanically tuning airDIBs, specific capacitance of oil-submerged droplets, normalized resistivity and specific capacitance plots, determination of osmotic pressured in droplets from electrolytes, plots of chemical potential and osmotic pressure, movies of formation, and thermal and mechanical manipulation of airDIBs. This material is available free of charge via the Internet at http://pubs.acs.org.

AUTHOR INFORMATION

Corresponding Author

*E-mail: colliercp@ornl.gov. Phone: +1 865 5763638. Fax: +1 865 5741753.

Author Contributions

The manuscript was written through the contributions of all authors. All authors have given approval to the final version of the manuscript.

Notes

The authors declare no competing financial interest.

ACKNOWLEDGMENTS

This manuscript has been authored by UT-Battelle, LLC, under contract no. DE-AC0500OR22725 with the U.S. Department of Energy. The United States Government retains and the publisher, by accepting the article for publication, acknowledges that the United States Government retains a nonexclusive, paid-up, irrevocable, worldwide license to publish or reproduce the published form of this manuscript, or allow others to do so, for the United States Government purposes. This research was conducted at the Center for Nanophase Materials Sciences, which is sponsored by Oak Ridge National Laboratory by the

DOI: 10.1021/la504712g
Langmuir XXXX, XXX, XXX−XXX

Scientific User Facilities Division, Office of Basic Energy Sciences, U.S. Department of Energy. Funding was provided by the Air Force Office of Scientific Research Basic Research Initiative grant FA9550-12-1-0464 (to S.A.S.) and by the SunShot Program of the Office of Energy Efficiency and Renewable Energy (to G.P.). We thank Kevin Lester and Bill McClintic for assistance with the experimental design.

REFERENCES

(1) Castellana, E. T.; Cremer, P. S. Solid Supported Lipid Bilayers: From Biophysical Studies to Sensor Design. *Surf. Sci. Rep.* **2006**, *61*, 429−444.
(2) Cheng, H. T.; London, E. Preparation and Properties of Asymmetric Large Unilamellar Vesicles: Interleaflet Coupling in Asymmetric Vesicles Is Dependent on Temperature but Not Curvature. *Biophys. J.* **2011**, *100*, 2671−2678.
(3) Funakoshi, K.; Suzuki, H.; Takeuchi, S. Lipid Bilayer Formation by Contacting Monolayers in a Microfluidic Device for Membrane Protein Analysis. *Anal. Chem.* **2006**, *78*, 8169−8174.
(4) Holden, M. A.; Needham, D.; Bayley, H. Functional Bionetworks from Nanoliter Water Droplets. *J. Am. Chem. Soc.* **2007**, *129*, 8650−8655.
(5) Sarles, S. A.; Leo, D. J. Physical Encapsulation of Droplet Interface Bilayers for Durable, Portable Biomolecular Networks. *Lab Chip* **2010**, *10*, 710−717.
(6) Sarles, S. A.; Leo, D. J. Regulated Attachment Method for Reconstituting Lipid Bilayers of Prescribed Size within Flexible Substrates. *Anal. Chem.* **2010**, *82*, 959−966.
(7) Punnamaraju, S.; Steckl, A. J. Voltage Control of Droplet Interface Bilayer Lipid Membrane Dimensions. *Langmuir* **2010**, *27*, 618−626.
(8) Dixit, S. S.; Pincus, A.; Guo, B.; Faris, G. W. Droplet Shape Analysis and Permeability Studies in Droplet Lipid Bilayers. *Langmuir* **2012**, *28*, 7442−7451.
(9) Hwang, W. L.; Holden, M. A.; White, S.; Bayley, H. Electrical Behavior of Droplet Interface Bilayer Networks: Experimental Analysis and Modeling. *J. Am. Chem. Soc.* **2007**, *129*, 11854−11864.
(10) Aghdaei, S.; Sandison, M. E.; Zagnoni, M.; Green, N. G.; Morgan, H. Formation of Artificial Lipid Bilayers Using Droplet Dielectrophoresis. *Lab Chip* **2008**, *8*, 1617−1620.
(11) Zagnoni, M.; Sandison, M. E.; Marius, P.; Morgan, H. Bilayer Lipid Membranes from Falling Droplets. *Anal. Bioanal. Chem.* **2009**, *393*, 1601−1605.
(12) Hwang, W. L.; Chen, M.; Cronin, B.; Holden, M. A.; Bayley, H. Asymmetric Droplet Interface Bilayers. *J. Am. Chem. Soc.* **2008**, *130*, 5878−5879.
(13) Leptihn, S.; Castell, O. K.; Cronin, B.; Lee, E.-H.; Gross, L. C.; Marshall, D. P.; Thompson, J. R.; Holden, M.; Wallace, M. I. Constructing Droplet Interface Bilayers from the Contact of Aqueous Droplets in Oil. *Nat. Protoc.* **2013**, *8*, 1048−1057.
(14) Verheijen, H.; Prins, M. Reversible Electrowetting and Trapping of Charge: Model and Experiments. *Langmuir* **1999**, *15*, 6616−6620.
(15) Krupenkin, T.; Yang, S.; Mach, P. Tunable Liquid Microlens. *Appl. Phys. Lett.* **2003**, *82*, 316−318.
(16) Quéré, D. Non-Sticking Drops. *Rep. Prog. Phys.* **2005**, *68*, 2495.
(17) Wong, T.-S.; Kang, S. H.; Tang, S. K.; Smythe, E. J.; Hatton, B. D.; Grinthal, A.; Aizenberg, J. Bioinspired Self-Repairing Slippery Surfaces with Pressure-Stable Omniphobicity. *Nature* **2011**, *477*, 443−447.
(18) Boreyko, J. B.; Polizos, G.; Datskos, P. G.; Sarles, S. A.; Collier, C. P. Air-Stable Droplet Interface Bilayers on Oil-Infused Surfaces. *Proc. Natl. Acad. Sci. U.S.A* **2014**, *111*, 7588−7593.
(19) Boreyko, J. B.; Mruetusatorn, P.; Sarles, S. A.; Retterer, S. T.; Collier, C. P. Evaporation-Induced Buckling and Fission of Microscale Droplet Interface Bilayers. *J. Am. Chem. Soc.* **2013**, *135*, 5545−5548.
(20) Mruetusatorn, P.; Boreyko, J. B.; Venkatesan, G.; Sarles, S. A.; Hayes, D.; Collier, C. P. Dynamic Morphologies of Microscale Droplet Interface Bilayers. *Soft Matter* **2014**, *10*, 2530−2538.
(21) Henn, F. A.; Thompson, T. E. Synthetic Lipid Bilayer Membranes. *Annu. Rev. Biochem.* **1969**, *38*, 241−262.
(22) Römer, W.; Steinem, C. Impedance Analysis and Single-Channel Recordings on Nano-Black Lipid Membranes Based on Porous Alumina. *Biophys. J.* **2004**, *86*, 955−965.
(23) White, S. H. Phase Transitions in Planar Bilayer Membranes. *Biophys. J.* **1975**, *15*, 95−117.
(24) White, S. H. Temperature-Dependent Structural Changes in Planar Bilayer Membranes: Solvent "Freeze-out. *Biochim. Biophys. Acta* **1974**, *356*, 8−16.
(25) White, S. H. A Study of Lipid Bilayer Membrane Stability Using Precise Measurements of Specific Capacitance. *Biophys. J.* **1970**, *10*, 1127−1148.
(26) Gross, L. C.; Heron, A. J.; Baca, S. C.; Wallace, M. I. Determining Membrane Capacitance by Dynamic Control of Droplet Interface Bilayer Area. *Langmuir* **2011**, *27*, 14335−14342.
(27) Schneider, C. A.; Rasband, W. S.; Eliceiri, K. W.; Schindelin, J.; Arganda-Carreras, I.; Frise, E.; Kaynig, V.; Longair, M.; Pietzsch, T.; Preibisch, S. 671 NIH Image to ImageJ: 25 Years of Image Analysis. *Nat. Methods* **2012**, *9* (7).
(28) Baba, T.; Toshima, Y.; Minamikawa, H.; Hato, M.; Suzuki, K.; Kamo, N. Formation and Characterization of Planar Lipid Bilayer Membranes from Synthetic Phytanyl-Chained Glycolipids. *Biochim. Biophys. Acta* **1999**, *1421*, 91−102.
(29) Sarles, S. A.; Leo, D. J. Tailored Current—Voltage Relationships of Droplet-Interface Bilayers Using Biomolecules and External Feedback Control. *J. Intell. Mater. Syst. Struct.* **2009**, *20*, 1233−1247.
(30) References23−26, as well as unpublished results by us, present specific capacitances that decrease slightly (by about 5%) over a wide temperature range (25 to 50 °C) due to uptake of hexadecane by the nonpolar hydrocarbon chains, which increases the effective bilayer thickness.
(31) Valincius, G.; Heinrich, F.; Budvytyte, R.; Vanderah, D. J.; McGillivray, D. J.; Sokolov, Y.; Hall, J. E.; Lösche, M. Soluble Amyloid-β-Oligomers Affect Dielectric Membrane Properties by Bilayer Insertion and Domain Formation: Implications for Cell Toxicity. *Biophys. J.* **2008**, *95*, 4845−4861.
(32) Gramse, G.; Dols-Perez, A.; Edwards, M.; Fumagalli, L.; Gomila, G. Nanoscale Measurement of the Dielectric Constant of Supported Lipid Bilayers in Aqueous Solutions with Electrostatic Force Microscopy. *Biophys. J.* **2013**, *104*, 1257−1262.
(33) Hung, W.; Chen, F.; Huang, H. W. Order−Disorder Transition in Bilayers of Diphytanoyl Phosphatidylcholine. *Biochim. Biophys. Acta* **2000**, *1467*, 198−206.
(34) Hsieh, C.-H.; Sue, S.-C.; Lyu, P.-C.; Wu, W. Membrane Packing Geometry of Diphytanoylphosphatidylcholine is Highly Sensitive to Hydration: Phospholipid Polymorphism Induced by Molecular Rearrangement in the Headgroup Region. *Biophys. J.* **1997**, *73*, 870−877.
(35) Disalvo, E.; Lairion, F.; Martini, F.; Tymczyszyn, E.; Frias, M.; Almaleck, H.; Gordillo, G. Structural and Functional Properties of Hydration and Confined Water in Membrane Interfaces. *Biochim. Biophys. Acta* **2008**, *1778*, 2655−2670.
(36) Sparr, E.; Hallin, L.; Markova, N.; Wennerström, H. Phospholipid-Cholesterol Bilayers under Osmotic Stress. *Biophys. J.* **2002**, *83*, 2015−2025.
(37) Milhaud, J. New Insights into Water−Phospholipid Model Membrane Interactions. *Biochim. Biophys. Acta* **2004**, *1663*, 19−51.
(38) Deamer, D. W.; Bramhall, J. Permeability of Lipid Bilayers to Water and Ionic Solutes. *Chem. Phys. Lipids* **1986**, *40*, 167−188.
(39) Rossignol, M.; Uso, T.; Thomas, P. Relationship between Fluidity and Ionic Permeability of Bilayers from Natural Mixtures of Phospholipids. *J. Membr. Biol.* **1985**, *87*, 269−275.
(40) White, S. H.; King, G. I. Molecular Packing and Area Compressibility of Lipid Bilayers. *Proc. Natl. Acad. Sci. U.S.A.* **1985**, *82*, 6532−6536.
(41) Scherer, J. R. The Partial Molar Volume of Water in Biological Membranes. *Proc. Natl. Acad. Sci. U.S.A.* **1987**, *84*, 7938−7942.

DOI: 10.1021/la504712g
Langmuir XXXX, XXX, XXX−XXX

(42) Blume, A.; Hillmann, M. Dimyristoylphosphatidic Acid/Cholesterol Bilayers. *Eur. Biophys. J.* **1986**, *13*, 343−353.
(43) Jendrasiak, G. L.; Smith, R. L. The Interaction of Water with the Phospholipid Head Group and its Relationship to the Lipid Electrical Conductivity. *Chem. Phys. Lipids* **2004**, 183−195.
(44) Heller, W. T.; He, K.; Ludtke, S. J.; Harroun, T. A.; Huang, H. W. Effect of Changing the Size of Lipid Headgroup on Peptide Insertion into Membranes. *Biophys. J.* **1997**, *73*, 239−244.
(45) Smith, G. S.; Sirota, E. B.; Safinya, C. R.; Plano, R. J.; Clark, N. A. Xray Structural Studies of Freely Suspended Ordered Hydrated DMPC Multimembrane Films. *J. Chem. Phys.* **1990**, *92*, 4519−4529.

DOI: 10.1021/la504712g
Langmuir XXXX, XXX, XXX−XXX